Electrochemical Properties of Electrodes Derived from $NaTi_3O_6OH \cdot 2H_2O$ in Sodium and Lithium Cells

Dhruv Seshadri,[a] Mona Shirpour,[*,b] and Marca Doeff[*,z]

Environmental Energy Technologies Division, Lawrence Berkeley National Laboratory, University of California at Berkeley, Berkeley, California 94720, USA

Materials derived from the layered compound $NaTi_3O_6OH \cdot 2H_2O$, also known as "sodium nonatitanate" or NNT, have recently been found to undergo reversible sodium or lithium intercalation processes at very low potentials. While practical discharge capacities in lithium cells can be above 200 mAh/g, making them of interest for high-energy applications, the presence of mobile sodium in the materials complicates the cycling behavior. A simple ion-exchange process prior to incorporation in electrochemical cells removes all sodium ions, producing the lithiated form of the material. The lithiated material (LNT) performs similarly to NNT in lithium cells, although coulombic inefficiencies are somewhat higher. A comparison is made between the behavior of NNT in sodium cells and that of NNT and the lithiated analog in lithium cells.

 [DOI: 10.1149/2.0391501jes]

Manuscript submitted September 12, 2014; revised manuscript received October 28, 2014. Published November 12, 2014. This was Paper 444 presented at the San Francisco, California, Meeting of the Society, October 27–November 1, 2013.

"Sodium nonatitanate" or NNT, which has long been used as an ion-exchanger for nuclear waste clean-up,[1] is identical to $NaTi_3O_6(OH) \cdot 2H_2O$, whose structure has recently been solved.[2] It consists of Ti_6O_{14} units linked together by corners and edges to form stacking faulted stepped layers, between which exchangeable sodium ions and water molecules are located (Figure 1a). Both the parent compound and a dehydrated form readily undergo electrochemical sodium and lithium insertion reactions at unusually low potentials; while reversibility is better for the anhydrous material than for the hydrated form in sodium cells, both types appeared to cycle reasonably well in lithium cells.[3] This presents an intriguing possibility of developing high-energy anodes based on NNT materials for lithium and sodium ion batteries, provided they could be developed further. The lower average insertion potential and higher theoretical capacity (~300 mAh/g) suggest that it could be a higher energy density alternative to the well-known anode material $Li_4Ti_5O_{12}$. Titanates are also denser materials than graphite, so full utilization of NNT in a Li-ion cell configuration should lead to a somewhat higher energy density (see reference 3 for more details).

The insertion processes and the causes of the high coulombic inefficiencies due to the very low potentials require further investigation, however. Another issue is that the presence of mobile sodium ions in the lithium ion system is undesirable from a performance and safety point of view. A recent NMR study[4] on composite electrodes derived from $NaTi_3O_6(OH) \cdot 2H_2O$ cycled in lithium cells showed evidence of in situ sodium plating during the discharge process. The observation suggests that mobile sodium ions underwent ion-exchange with the electrolytic solution and/or were de-intercalated upon recharge, then subsequently were reduced to metallic sodium at the very low potentials encountered during later discharges. This phenomenon provided the impetus for the current study, in which the physical and electrochemical properties of lithium ion-exchanged versions of sodium nonatitanate are described and compared to those of the unexchanged starting materials.

Experimental

$NaTi_3O_6(OH) \cdot 2H_2O$ (sodium nonatitanate or NNT) was synthesized hydrothermally according to the procedure outlined in reference 3. The anhydrous form of NNT, used in some of the experiments, was produced by drying the as-made material at 600°C for two hours and is designated anh-NNT.

For the ion exchange procedure, NNT was dried and ground to create a homogenous powder. One gram was added to a 4M $LiNO_3$ aqueous solution and stirred at 80°C for 6 days to facilitate ion exchange. The solution was then allowed to cool to room temperature and was consequently filtered, washed, and dried in a vacuum oven overnight at 120°C. The resulting compound is designated LNT. A portion of this was heated to 600°C for one hour in an attempt to further remove water.

X-ray diffraction (XRD) patterns were obtained using a Bruker D2-Phaser diffractometer and CuKα radiation (λ = 1.54178 Å). Lattice parameters were determined by profile matching with constant scale factor (LeBail fit) using the WinPLOTR/Fullprof Suite[5] for NNT. Scanning Electron Microscopy (SEM) images were obtained using a JEOL JSM-7500 field emission microscope. Energy dispersive X-ray spectroscopy (EDS) data were collected using a Noran system S1X (Thermo Electron Corporation, model 6714A01SUS-SN) probe attached to the SEM. NNT was used as a reference and the LNT sample was analyzed to monitor the sodium ion content.

Composite electrodes were prepared by making a slurry of 70 wt% active material, 25 wt% of acetylene black (Denka, 50% compressed), and 5 wt% polyvinylidene difluoride (PVDF) (99.5+%, Sigma Aldrich) in N-methyl-2-pyrolidinone (NMP, Sigma Aldrich). The active material and the acetylene black were first mixed together in a planetary mill for two hours at 300 rpm. The resulting slurry was cast on copper foil that had been lightly etched to improve adhesion for use in lithium cells, or Al foil for use in sodium cells. The laminate was then dried under a heat lamp for about an hour and electrodes were cut to size and weighed. Their typical thickness was approximately 60 μm and the loading was about 5 mg/cm^2. Size 2032 coin cells were assembled in a He-filled glove box using the composite electrodes, Celgard 2400 separators, 1M LiPF6 in EC/DMC 1:2 (Novolyte Technologies) as the electrolytic solution and lithium foil electrodes for the lithium cells. For sodium cells, sodium foils made by extruding sodium ingots were used as anodes, and a solution made in-house of 1 M $NaPF_6$ (Sigma-Aldrich) in ethylene carbonate–dimethylene carbonate (EC : DMC) 3 : 7 mol (from Novolyte Technologies) was used as the electrolytic solution. Cells were cycled at room temperatures under various conditions using a Bio-Logic VMP3 potentiostat/galvanostat.

Partially and fully discharged and recharged electrodes were harvested from sodium and lithium coin cells for synchrotron XRD experiments at beam line 11–3 at the Stanford Synchrotron Radiation Lightsource. Prior to the experiment, the electrodes were scraped from

[*]Electrochemical Society Active Member.
[a]Present address: Department of Biomedical Engineering, Texas A&M University, College Station, Texas 77843-1372, USA.
[b]Present address: Department of Chemical & Materials Engineering, University of Kentucky, Lexington, Kentucky 40506, USA.
[z]E-mail: mmdoeff@lbl.gov

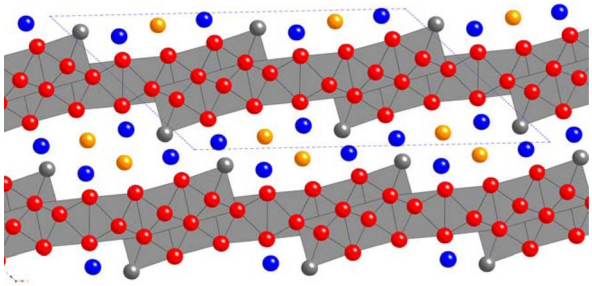

Figure 1. Structure of $NaTi_3O_6OH \cdot 2H_2O$ (NNT) consisting of TiO_6 octahedral units (gray) linked by corners and edges to form stepped layers. Sodium ions (orange spheres) and water molecules (blue spheres represent oxygens of H_2O) are located between the galleries. Oxygen in TiO_6 units and those belonging to OH groups on steps are represented by red and gray spheres, respectively.

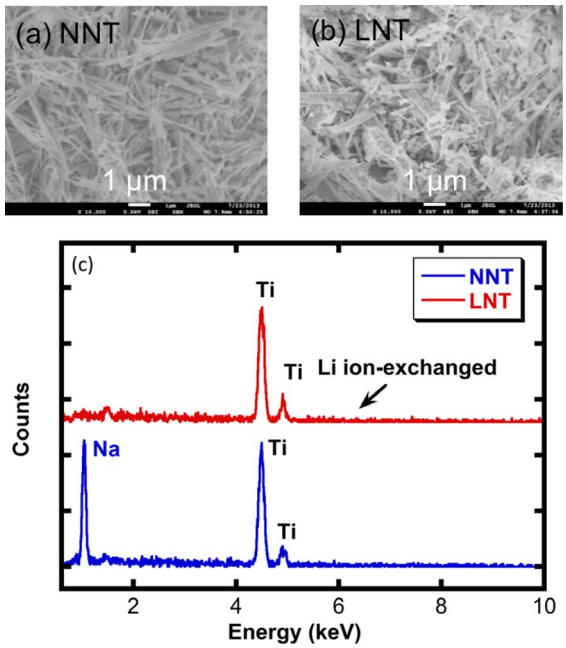

Figure 2. SEM images of (a) NNT and (b) LNT, and (c) EDS analysis of NNT (bottom) and LNT (top) indicating complete removal of sodium for the latter.

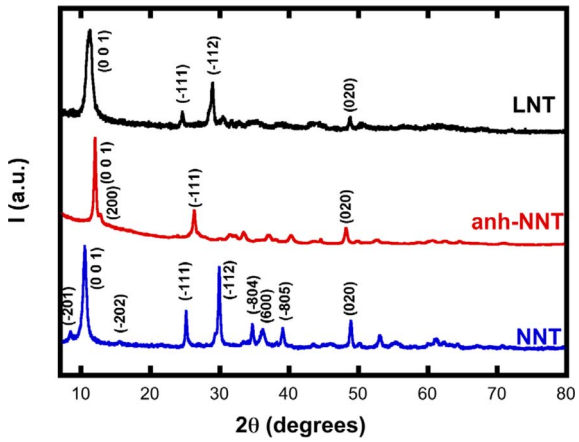

Figure 3. XRD powder patterns of (bottom) NNT, (middle) anh-NNT, and (top) LNT.

Table I. Structural parameters of compounds derived from $NaTi_3O_6OH \cdot 2H_2O$ (NNT), space group C2/m.

Sample	interlayer spacing, Å[b]	*a*, Å	*b*, Å	c, Å	β, °
NNT[a]	8.41	21.50	3.74	11.88	136.13
anh-NNT	7.37	N/A	N/A	N/A	N/A
LNT	7.73	N/A	N/A	N/A	N/A

[a]determined from full refinement (reference 3).
[b]from 001 d-spacing (see Figure 1).

the current collectors, mounted on aluminum substrates, and covered with Kapton to protect them from air.

Results and Discussion

As-made $NaTi_3O_6OH \cdot 2H_2O$ (NNT) exhibits a nanoribbon particle morphology (Figure 2a), which is retained in the anhydrous form and in the ion-exchanged version of the material, LNT (Figure 2b). EDS analysis indicates that no sodium was present in LNT after the ion-exchange and drying treatments (Figure 2c). Based on this observation, we can reasonably assume that all of the sodium was replaced by lithium during the ion exchange process.

XRD patterns for NNT, anh-NNT, and LNT are given in Figure 3, with the major reflections indexed for each phase. Dehydration of NNT under the treatment conditions used for this study removed all the interlayer water and resulted in a shift of the 001 reflection in the anh-NNT pattern to higher values of 2θ, consistent with a decrease in the interlayer spacing compared to the original compound (Figure 1, Table I). The XRD patterns of anh-NNT and NNT are similar, indicating that the gross structural features are maintained during the dehydration processes. Besides the change in the interlayer spacing, there is a decrease in the intensity of the (-112) reflection in the pattern of anh-NNT compared to that of NNT, due to removal of water and rearrangement of ions in the interlayer space. The detailed structure of this compound has not been solved, but a Raman study[2] of the dehydration process indicated that connecting O-Na-O or O-H-O bonds form as water is lost from NNT, so that a pseudo-tunnel structure is generated (Figure 4).

The XRD pattern of LNT resembles that of NNT, although the peaks are substantially broader than those of either NNT or anh-NNT, indicative of increased disorder. There is also a systematic absence or attenuation of the *h*0*l* reflections. This is consistent with the replacement of the heavier sodium ions between the galleries with lighter lithium ions, as well as an increased number of stacking faults. The interlayer spacing is smaller than that for NNT but larger than in anh-NNT suggesting that some interlayer water is still present in LNT. An attempt to dry the metastable LNT by heating it at 600°C for one hour

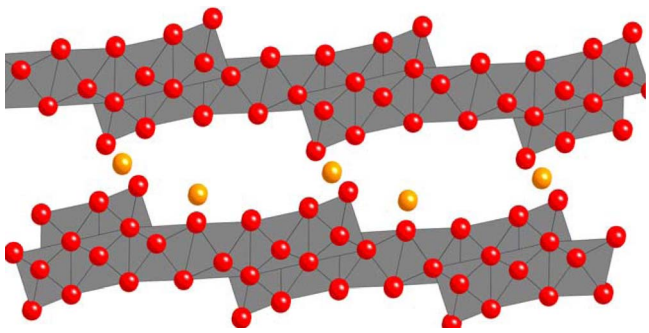

Figure 4. Proposed structure of anh-NNT. The stepped layers of corner and edge-shared TiO_6 octahedral units (gray) are identical to those found in NNT. Na or H ions (orange spheres) form links between the steps so that a pseudo-tunnel structure is formed.

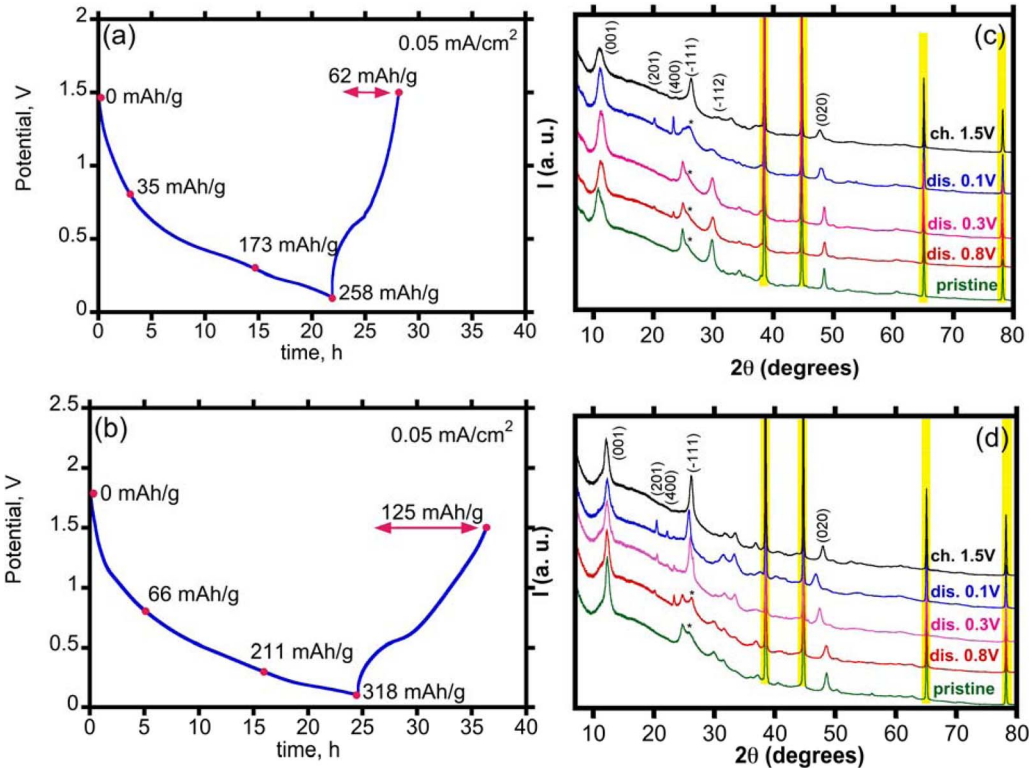

Figure 5. Voltage profiles of (a) Na/NNT (top left) and (b) Na/anh-NNT (bottom left) cells from which electrodes were harvested (at the points indicated by red dots) to obtain the ex situ synchrotron XRD patterns shown on the top right (c, NNT electrodes) and the bottom right (d, anh-NNT electrodes). Reflections from the Al substrates are highlighted in yellow, and asterisks mark weak reflections from Kapton films used to protect electrodes from the atmosphere. A carbon conductive additive and PVdF binder also contribute background to the patterns.

resulted in complete conversion to Li_2TiO_3; for this reason all of the electrochemistry was performed on LNT dried at 120°C.

To better understand the electrochemical behavior of the NNT materials, several Na/NNT and Na/anh-NNT cells were assembled, and discharged or recharged to various voltage limits as indicated by the red dots on the voltage profiles shown in Figure 5. Note that in this study, which utilized half-cells with either metallic lithium or sodium anodes, we refer to electrochemical sodiation or lithiation of NNT as discharge, and desodiation or delithiation as charge. Because Ti is initially in the +4 oxidation state in the as-made materials, it is not likely that an initial charge (desodiation or delithiation) could be carried out without damaging the electrode; for this reason, cells were always started on discharge.

Electrodes were then harvested from the partially or fully discharged and recharged cells to obtain ex situ synchrotron XRD diffraction patterns. Both NNT and anh-NNT exhibit sloping discharge profiles characteristic of solid solution and/or pseudo-capacitative processes. The initial discharges are complicated by irreversible side reactions such as insertion of sodium ions into the carbon additive, and solid electrolyte interface (SEI) formation.[6] (See Figure S2 in the supplemental information provided with reference 3 for data obtained on blank carbon electrodes showing evidence of electroactivity in sodium and lithium half-cells). The cycling behavior of sodium half-cells containing anh-NNT is much better than that of those with NNT electrodes; although the first cycle coulombic inefficiency is high due to the aforementioned side reactions, capacity retention thereafter is good.

The XRD patterns of the NNT electrodes changed as a function of state-of-charge, indicating that the redox processes involve participation of the bulk material rather than the particle surfaces alone (i.e., pseudocapacitance). The patterns of the discharged and recharged electrodes still resemble that of the pristine material, indicating that they are structurally related. The very weak (201) and (400) reflections, which were undetectable in the pristine electrode, progressively grew in intensity as the discharge progressed, and then disappeared again in the pattern of the recharged electrode. These lattice planes intersect the van der Waals gaps so that this observation is consistent with insertion of sodium ions into specific sites between the titanate layers during discharge. Full or partial occupancies of the sites by the relatively high z sodium ions caused the intensities of these reflections to increase in the discharged electrodes, and their removal decreased the intensities again. In addition, the (001) peaks shifted slightly rightward, indicating that the interlayer spacing became smaller as the discharge progressed, reaching a value of about 7.8 Å in the fully discharged electrode. Upon recharge, the interlayer spacing increased to 7.95 Å, smaller than the value of 8.41 Å found in the pristine material. The amount of intercalated sodium likely influences the size of the interlayer spacing, but it has also been found to be highly sensitive to the interlayer water content.[3,7] The smaller interlayer spacing found in the recharged electrode suggests strongly that the interlayer water content was reduced during cycling; i.e. intercalation of sodium displaced interlayer water, as has also been observed in lepidocrocite-structured titanate anodes during cycling in sodium cells.[8] Further evidence for this is the greatly reduced intensity of the (-112) reflection observed in the recharged electrode; in this, the XRD pattern more closely resembles that of anh-NNT rather than pristine NNT itself, except that the interlayer spacing is somewhat greater.

These results imply that interlayer water in the as-made NNT is released into the electrolytic solution. Because of the low operating potentials of these cells, it is likely that it is reduced to hydrogen, as has been observed in Li-ion cells with $Li_4Ti_5O_{12}$ anodes, to which water was deliberately added.[9] Somewhat surprisingly, the addition of small amounts of water (up to 2000 ppm) to the Li-ion cells in reference 9 did not have an adverse impact on the cycling behavior, although side reactions involving $LiPF_6$ and water are known to

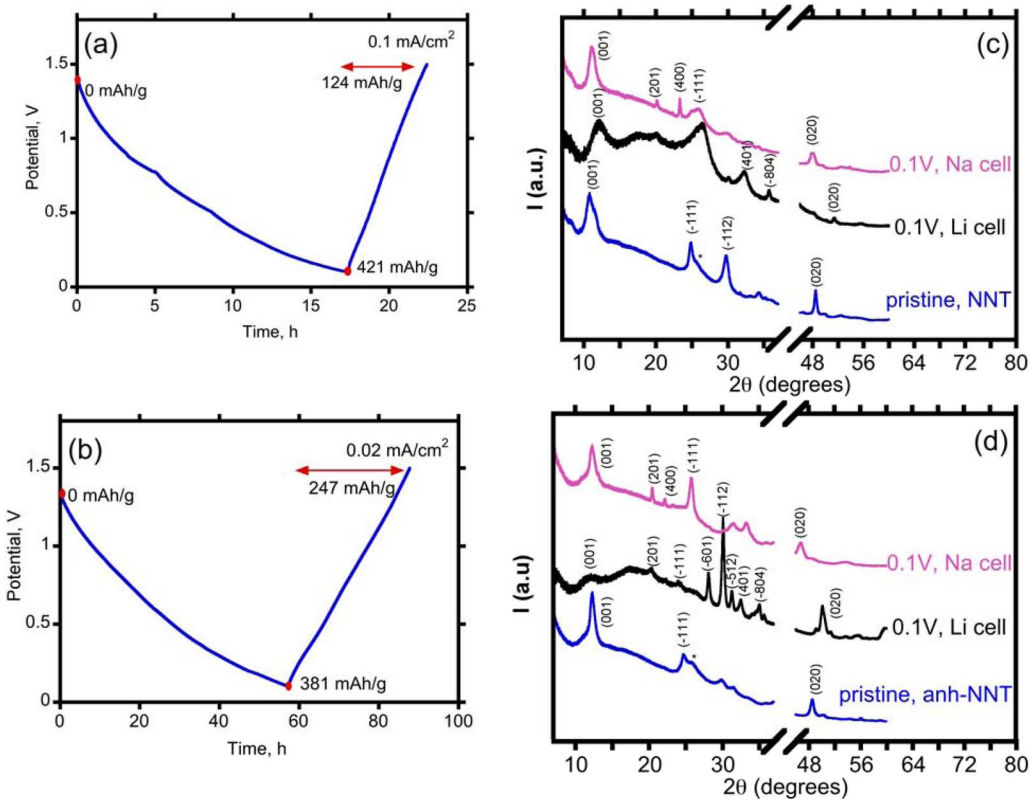

Figure 6. Voltage profiles of (a) Li/NNT (top left) and (b) Li/anh-NNT (bottom left) cells from which discharged electrodes were harvested at 0.1 V (indicated with the red dot). The ex situ synchrotron XRD patterns of the pristine and discharged electrodes, along with the pattern of the electrode discharged in a sodium cell are shown on the top right (c, NNT electrodes) and the bottom right (d, anh-NNT electrodes). For better clarity, peaks from the Al substrates were removed and the data was normalized to the strongest peak belonging to the active material. Asterisks mark weak reflections from Kapton films used to protect electrodes from the atmosphere. A carbon conductive additive and PVdF binder also contribute background to the patterns.

occur.[10] The impact of water on sodium-ion cell performance is, as yet, unknown and needs to be assessed.

The absence of reflections that can be assigned to other phases not related to NNT or electrode components suggests that phase degradation during cycling is not the cause of the poor cycling behavior for this material, although partial decomposition to an amorphous product cannot be completely ruled out by this experiment. The cooperative displacement of water by sodium and the volume changes associated with intercalation processes may cause disconnection of active particles in the composite electrodes, leading to the observed irreversibility.

Similar phenomena are observed in the XRD patterns of the discharged and recharged anh-NNT electrodes taken from sodium cells (Figure 5) and likewise are characteristic of sodium intercalation processes. As with the NNT electrodes, the (201) and (400) reflections, normally weak or undetectable in the pristine powders, increased in intensity in the patterns of the partially or fully discharged electrodes and disappeared for the recharged electrode. Shifting of the (001) reflections as the discharge progressed is less evident for the anh-NNT electrodes than in the case of NNT, and the value of the interlayer spacing in the recharged electrode is close to that of the pristine material (7.32 Å vs. 7.37 Å), indicating better reversibility for the anh-NNT electrode. The changes in the position of the (020) reflection for electrodes with state-of-charge indicates that the sodium insertion processes strongly affect the *b*-lattice parameter; however it was not possible to determine these changes as a function of composition due to uncertainties both with the structural details and with the exact state-of-charge due to the first cycle side reactions.

Figure 6 compares the patterns of NNT and anh-NNT electrodes discharged in lithium cells with the pristine electrodes and electrodes discharged in sodium cells. For better clarity, regions of the patterns obscured by the Al foil substrates were omitted and the data was normalized to the strongest peak in the active material phase. The voltage profiles of Li/NNT and Li/anh-NNT cells are also provided for reference. As with the sodium half-cells, the discharge profiles of NNT and anh-NNT are sloping, suggestive of single-phase processes. Irreversible side reactions also contribute capacity to the initial discharges, resulting in high first cycle coulombic inefficiencies, but capacity retention thereafter is reasonably good. Unlike in the sodium cells, the NNT material cycles nearly as well as the anh-NNT electrode, although the reversible capacities are lower and the first cycle coulombic inefficiencies are higher.

Most of the peaks in the pattern of the NNT electrode discharged to 0.1 V in a lithium half cell are markedly broader than those in the patterns of the pristine electrode and the one discharged to 0.1 V in a sodium cell. This is indicative of greatly increased disorder in the lithiated NNT phase compared to the sodiated and pristine ones. In contrast, many of the reflections observed in the pattern of the lithiated anh-NNT electrode are sharper and more intense, although the low-angle (001) peak is extremely broad and diffuse, to the point where it is barely detectable. This implies that there is a wide variation of interlayer spacings in a single lithiated phase, as may occur if sodium and lithium ions are distributed unevenly among the galleries. This could happen if partial ion exchange occurred between the active material and the electrolytic solution during the course of the slow discharge so that some of the original sodium present in the starting material was randomly replaced with lithium. Both the broad (001) peaks in the lithiated anh-NNT and NNT electrodes are centered at about 7.32 Å, suggesting that the interlayer water in NNT was displaced by the inserted alkali metal ions during the discharge process, as was also the case for the sodiation reaction. The combination of lithium intercalation, partial ion exchange, and water displacement clearly complicates

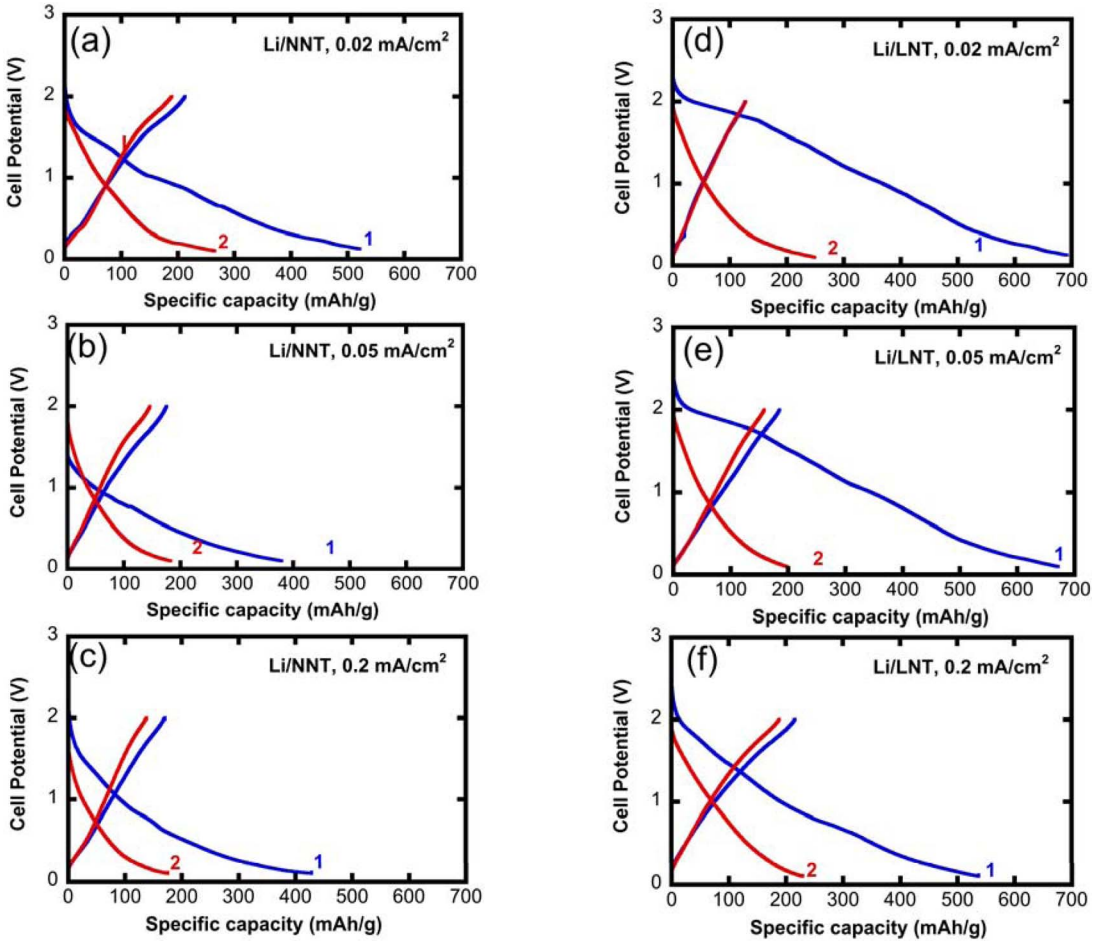

Figure 7. Voltage profiles of the first two cycles of (left) Li/NNT cells discharged at 0.02 mA/cm^2 or C/50 (a), 0.05 mA/cm^2 or C/20 (b), and 0.2 mA/cm^2 or C/5 (c) and (right) Li/LNT cells discharged at 0.02 mA/cm^2 or C/50 (d), 0.05 mA/cm^2 or C/20 (e), and 0.2 mA/cm^2 or C/5 (f) between 2.0–0.1 V.

the discharge processes in NNT, resulting in a very disordered lithiated product in which sodium and lithium ions are distributed over many types of sites between the titanate layers. In contrast, lithiation of anh-NNT yields a product, which, although it is disordered along the *c*-axis, contains alkali metal cations in specific sites, judging by the intensification of relatively sharp mid-angle peaks involving lattice planes that intersect the interlayer spacing.

The ex situ synchrotron XRD experiments on NNT and anh-NNT in lithium cells imply that ion exchange occurs when electrodes are in contact with electrolytic solutions containing lithium salts. Numerous layered titanate structures have been observed to undergo ion-exchange processes readily, including $Na_2Ti_3O_7$,[11,12] lepidocrocite titanates such as $K_{0.8}[Ti_{1.73}Li_{0.27}]O_4$,[13] and NNT[1,14] itself. Ex situ ion exchange has been used to prepare metastable analogs of the parent titanates for study in alkali metal cells; e.g., $Li_2Ti_3O_7$ from $Na_2Ti_3O_7$[15,16] and $Na_{0.8}[Ti_{1.73}Li_{0.27}O_4]$ from $K_{0.8}[Ti_{1.73}Li_{0.27}]O_4$.[8] It is therefore not too surprising that this can occur when NNT is exposed to a lithium salt-containing electrolytic solution.

Further evidence for in situ ion exchange is given by recent ^{23}Na MAS-NMR experiments on NNT electrodes discharged and cycled to 0.1 V vs. Li^+/Li, showing a signal attributable to the presence of metallic sodium.[4] As the in situ ion exchange occurred in the lithium cell, sodium ions from the NNT were released into the electrolytic solution. The voltages encountered during cell discharge were below the sodium plating potential, which is -2.71 V vs. S. H. E.[17] or about +0.3 V vs. Li^+/Li, so that metallic sodium readily formed. Although "hybrid ion" cells have been proposed, in which sodium-containing materials are cycled in a lithium ion battery configuration,[18,19] these results suggest that caution should be used with this approach. Even if the materials themselves do not undergo redox reactions at low potentials, sodium ions released into the electrolytic solution via ion exchange may migrate to the anode, resulting in sodium plating there. Because this is an unsafe situation, it would be preferable to remove sodium ions from electroactive materials prior to incorporation in lithium ion cells intended for commercial use.

Because LNT does not contain sodium, it is a better candidate for use in lithium cells than NNT. However, it was not known whether the chemical ion exchange and the inevitable presence of interlayer water, due to difficulties in drying LNT, would change the electrochemical behavior. To determine this, Li/NNT and Li/LNT cells were assembled and cycled at different rates between 2.0–0.1 V. Figure 7 shows the first two cycles of three sets of each type of cells, discharged and charged at 0.02, 0.05, and 0.2 mA/cm^2 (corresponding to roughly C/50, C/20, and C/5 rates). All of the cells showed high first cycle inefficiencies, but those for the LNT cells were inversely dependent on the cycling rates, while those for the NNT cells remained fairly constant. The shapes of the first discharge profiles for the LNT cells were also somewhat different than those of NNT, particularly at the two lower rates. It is possible that residues left over from the ion exchange process on particle surfaces either catalyzed or contributed to side reactions, resulting in greater first cycle irreversibilities for the LNT cells. Better reversibility was observed during the second cycles of all of the cells, and the voltage profiles all appeared similar; i.e., gradually sloping and featureless, typical of solid solution processes. The second cycle discharge capacities of both materials exceeded 250 mAh/g at the lowest current density, and decreased modestly at

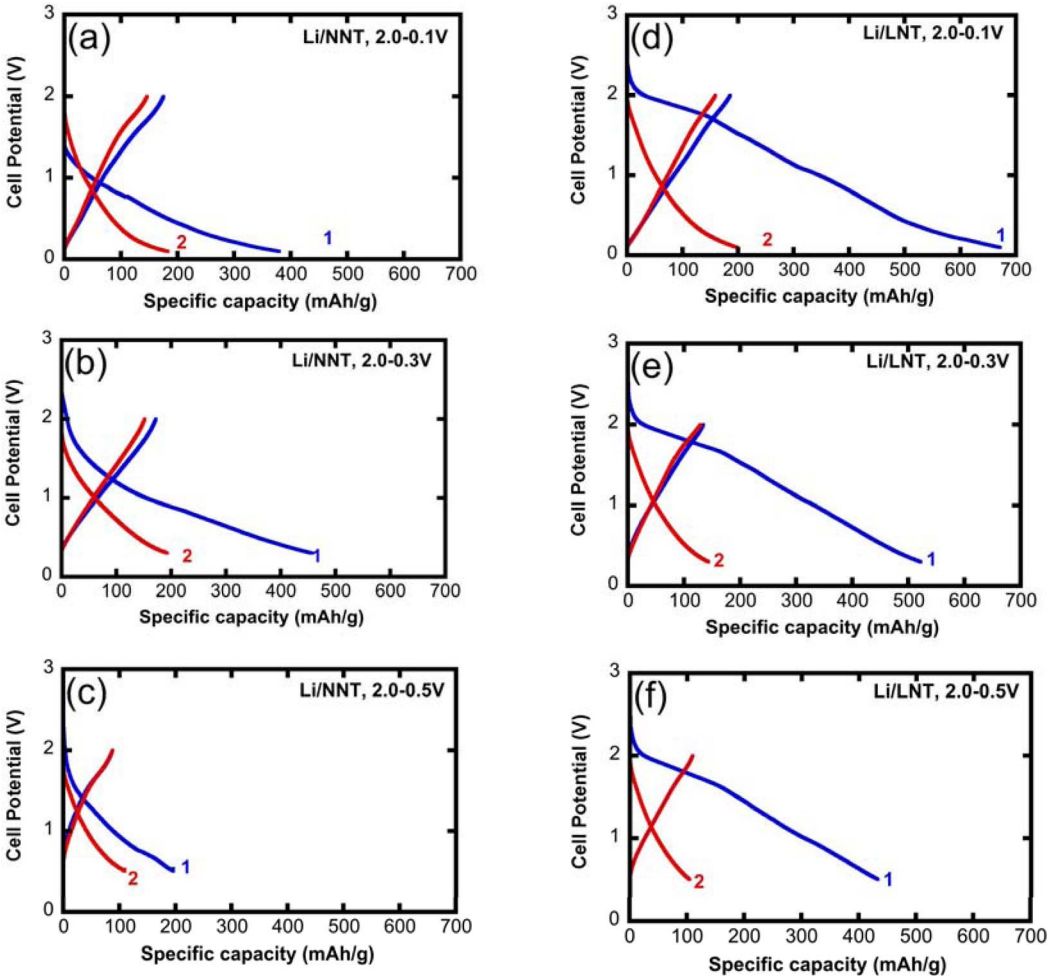

Figure 8. Voltage profiles of the first two cycles of (left) Li/NNT cells discharged at 0.05 mA/cm^2 or C/20 between 2.0–0.1 V (top), 2.0–0.3 V (middle), and 2.0–0.5 V (bottom) and (right) Li/LNT cells discharged at 0.05 mA/cm^2 or C/20 between 2.0–0.1 V (top), 2.0–0.3 V (middle), and 2.0–0.5 V (bottom).

the higher rates. Interestingly, the lowest capacity was obtained at the intermediate rate for the Li/LNT cells rather than the lowest, implying a competition occurred between the side reactions and the intercalation reaction, which occur at different rates. At higher current densities, intercalation outpaced the side reactions, resulting in better efficiency and more complete utilization of the electrode. At the lowest rate, both the side reactions and the intercalation process contributed, resulting in high inefficiency but also better reversible capacity (judging from the second cycle) than in the cell discharged at the intermediate rate.

In an effort to reduce the first cycle coulombic inefficiency, the effect of the lower voltage limit was studied on Li/NNT and Li/LNT cells cycled at 0.05 mA/cm^2 ($\sim$ C/20, Figure 8). Raising this limit primarily affected the second cycle discharge capacity rather than the first cycle efficiency; increasing it to 0.5 V lowered the capacities in both types of cells to almost half of the value obtained when a 0.1 V limit was used. The reduction in capacity was less apparent in the cells cycled to 0.3 V, however. In all cases, the first cycle coulombic inefficiencies (defined as the capacities of the first charges divided by the capacities of the first discharges) remained constant at about 45% for the NNT cells and less than 30% for the LNT cells, regardless of the voltage limit used. The side reactions appear to take place over a wide voltage window, making it difficult to reduce them by manipulating the voltage window. To improve the first cycle reversibility, effort should instead be directed toward active material particle engineering (e.g., reduction of surface area) and electrode engineering (reduction of carbon content, use of more compliant binders, additives etc.). The release of interlayer water from the hydrated electrodes into the system during cell cycling probably also contributed to the high first cycle irreversibility, because it is most likely reduced to hydrogen gas irreversibly. The fact that first cycle coulombic efficiencies were better for Li/anh-NNT cells than for Li/NNT cells provides further evidence for this.[3] If it is possible to prepare anhydrous LNT, either by ion-exchanging anh-NNT using a nonaqueous process, or by carefully drying LNT at temperatures low enough to prevent the phase change to Li_2TiO_3, this should improve first cycle efficiencies in the cells.

Cycling data is shown in Figures 9 and 10 for Li/NNT and Li/LNT cells. Capacity retention was good over 30 cycles, with some cells achieving in excess of 150 mAh/g (e.g., Li/LNT cell at 0.2 mA/cm^2 or C/5). Efficiencies improved greatly after the first cycle, generally approaching 100% within a few cycles, although this was dependent on the rate used (Figure 9), particularly for Li/LNT cells. The poor cycling efficiency of the Li/LNT cell at the lowest current density also explains why the capacity retention is lower than for the cells cycled at higher rates and suggests that SEI formation is incomplete under these conditions. Cycling capacities were affected by the lower voltage limit used in both the Li/NNT and Li/LNT cells (Figure 10), decreasing as this value was raised. There was relatively little effect of voltage limit on efficiencies during later cycles for the Li/NNT cells. For the Li/LNT cells, even though the voltage limit used did not affect the magnitude of the first cycle inefficiencies, it did influence them somewhat on subsequent cycles. The improvement of the overall cycling efficiency was not enough to offset the decrease in capacity associated with higher voltage limits, however.

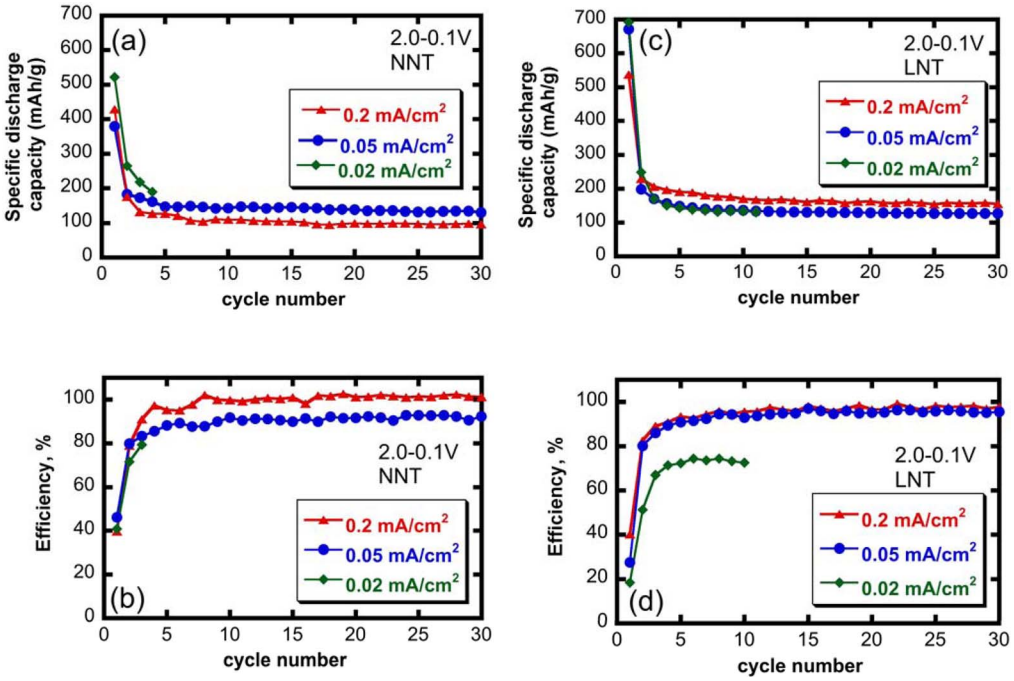

Figure 9. Cycling capacities (a) and efficiencies (b) for Li/NNT cells and for Li/LNT cells (c, d) as a function of current densities between 2.0–0.1 V.

The electrochemical characteristics of LNT in lithium cells clearly resemble those of NNT in several key aspects; in particular, the low potentials at which lithium insertion occurs and the sloping discharge curves associated with solid solution processes. Discharge capacities and capacity retentions of Li/LNT cells were similar to those of Li/NNT cells, but both first cycle and subsequent cycle coulombic efficiencies were somewhat higher, and were sensitive to both current density and the voltage window used. Both NNT and LNT contain interlayer water, which is probably reduced during the first discharge, and contributes to inefficiency, primarily in early cycles. The behavior during subsequent cycles suggests that there were some subtle differences between the NNT and LNT materials that resulted in increased and more persistent side reactions. Besides a possible contribution of residue left over from the chemical exchange process, changes in physical characteristics, such as increased surface area, may have led to less efficient passivation processes in the LNT electrodes. Nevertheless, the demonstration of initial capacities in excess of 200 mAh/g at average potentials of just 0.5 V vs. Li^+/Li for these relatively dense materials (~3.5 g/cc) indicate that high energy densities may be achievable for this system. Further work should be directed toward improving the ion exchange process, optimizing particle morphologies, and engineering better composite

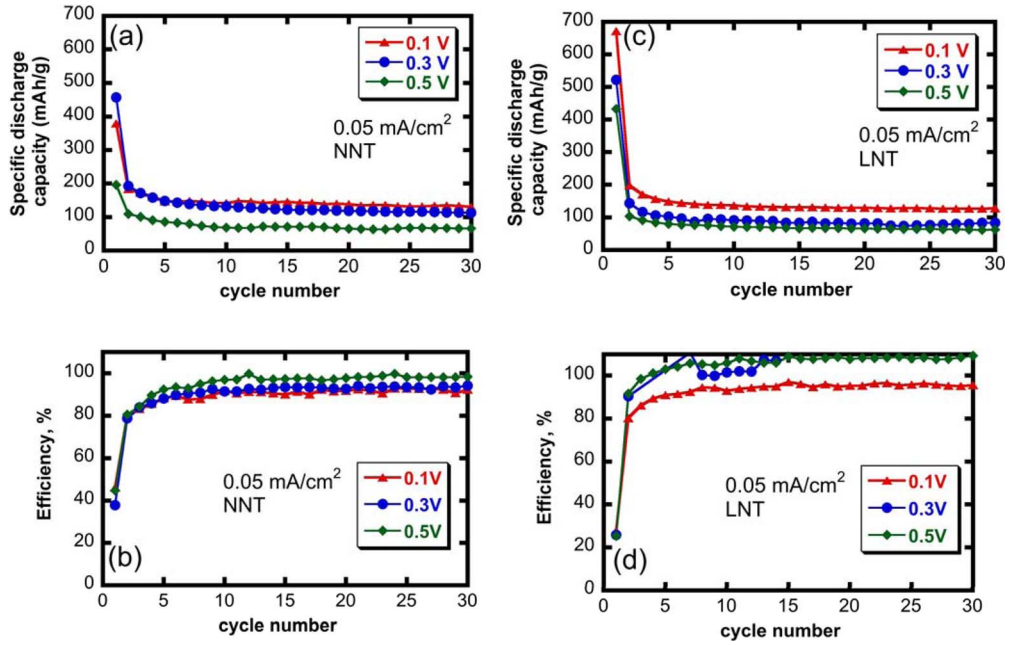

Figure 10. Cycling capacities (a) and efficiencies (b) for Li/NNT cells and for Li/LNT cells (c, d) at 0.05 mA/cm^2 (C/20) between 2.0 and the indicated lower voltage limits.

electrodes, so that coulombic inefficiencies are minimized in the LNT material.

Conclusions

The electrochemical characteristics of electrodes based on $NaTi_3O_6OH \cdot 2H_2O$ (NNT) have been studied. Ex situ synchrotron X-ray diffraction experiments show that both NNT and the anhydrous form (anh-NNT) undergo electrochemical lithium and sodium intercalation reactions during discharge. The reactions are reversible, although interlayer water is displaced by the intercalated alkali metal ions. Lithium insertion results in significantly more disorder in the reduced NNT and anh-NNT phases than sodium insertion does, particularly for NNT. This is partially due to in situ ion exchange processes occurring in electrodes in cells undergoing discharge, resulting in a distribution of interlayer spacings within the same phase. Because of safety concerns associated with the release of sodium ions into the electrolytic solution and the possibility of sodium plating at the low potentials encountered during discharge, a Li-ion exchanged version of NNT (LNT) was prepared, and its discharge characteristics were compared to that of NNT. Like NNT, LNT exhibits a sloping voltage profile with a low average discharge potential of about 0.5 V in lithium cells. Initial discharge capacities in excess of 200 mAh/g were observed for both NNT and LNT electrodes in lithium cells, implying that energy densities could be quite high for these materials. Both LNT and NNT electrodes appear to cycle with good capacity retention, although coulombic inefficiencies were generally higher for cells containing LNT. Suggestions are made for decreasing inefficiencies by improving ion exchange processes, optimizing particle morphologies and better engineering of electrodes.

Acknowledgments

This work was supported by the Laboratory Directed Research and Development Program of Lawrence Berkeley National Laboratory under U.S. Department of Energy Contract DE-AC02- 05CH11231. Portions of this research were carried out at the Stanford Synchrotron Radiation Lightsource, a Directorate of SLAC National Accelerator Laboratory and an Office of Science User Facility operated for the U.S. Department of Energy Office of Science by Stanford University. D.S. thank the Science Undergraduate Laboratory Internship (SULI) program sponsored by the U.S. Department of Energy for a summer internship spent at Lawrence Berkeley National Laboratory.

References

1. J. Lehto and A. Clearfield, *J. Radioanal. Nucl. Chem. Lett.*, **118**, 1 (1987).
2. I. Andrusenko, E. Mugnaioli, T. E. Gorelik, D. Koll, M. Panthoefer, W. Tremel, and U. Kolb, *Acta Crystallogr., Sect. B: Struct. Sci*, **67**, 218 (2011).
3. M. Shirpour, J. Cabana, and M. Doeff, *Energy Environ. Sci.*, **6**, 2538 (2013).
4. Mallory Gobet, PhD thesis, Department of Physics and Astronomy, Hunter College of CUNY, New York, 2014.
5. J. Rodriguez-Carvajal, *Physica B*, **192**, 55 (1993). (WinPLOTR software at http://www-llb.cea.fr/fullweb/winplotr/winplotr.htm.).
6. P. Senguttuvan, G. Rousse, V. Seznec, J.-M. Tarascon, and M. Rosa Palacin, *Chem. Mater.*, **23**, 4109 (2011).
7. P. Sylvester, T. Moller, T. W. Adams, and A. Cisar, *Appl. Radiat. Isot.*, **61**(6), 1139 (2004).
8. M. Shirpour, J. Cabana, and M. Doeff, *Chem. Mater.*, **26**(8), 2502 (2014).
9. J. C. Burns, N. N. Sinha, Gaurav Jain, Hui Ye, Collette M. VanElzen, Erik Scott, A. Xiao, W. M. Lamanna, and J. R. Dahn, *J. Electrochem. Soc.*, **161**, A247 (2014).
10. D. Aurbach, B. Markovsky, G. Salitra, E. Markevich, Y. Talyossef, M. Koltypin, L. Nazar, B. Ellis, and D. Kovacheva, *J. Power Sources*, **165**, 491 (2007).
11. Y. An, D. Wang, and C. Wu, *Physica E*, **60**, 210 (2014).
12. H. Izawa, S. Kikkawa, and M. Koizumi, *J. Phys. Chem.* **86**, 5023 (1982).
13. T. Sasaki, F. Kooli, M. Iida, Y. Michiue, S. Takenouchi, Y. Yajima, F. Izumi, B. C. Chakoumakos, and M. Watanabe, *Chem. Mater.* **10**, 4123 (1998).
14. S. F. Yates and P. Sylvester, *Sep. Sci. and Tech.*, **36**, 867 (2001).
15. K. Chiba, N. Kijima, Y. Takahashi, Y. Idemoto, and J. Akimoto, *Solid State Ionics*, **178**, 1725 (2008).
16. G. Rousse, M. E. Arroyo-de Dompablo, P. Senguttuvan, A. Ponrouch, J.-M. Tarascon, and M. R. Palacín, *Chem. Mater.*, **25**, 4946 (2013).
17. *CRC Handbook of Chemistry and Physics*, 89th ed.; D. R. Lide, Ed.; CRC Press: Boca Raton, FL, Section 3, No. 339 (2008).
18. J. Barker, R. K. B. Gover, P. Burns, and A. J. Bryan, *Electrochem. Solid State Lett.*, **9**, A190 (2006).
19. B. L. Ellis, W. R. M. Makahnouk, Y. Makimura, K. Toghill, and L. F. Nazar, *Nature Mater.* **6**, 749 (2007).